Available online at www.sciencedirect.com
SCIENCE DIRECT
Geochimica et Cosmochimica Acta 70 (2006) 1695–1709
Geochimica
www.elsevier.com/locate/gca

Pleistocene chemical weathering history of Asian arid and semi-arid regions recorded in loess deposits of China and Tajikistan

Shiling Yang *, Feng Ding, Zhongli Ding

Institute of Geology and Geophysics, Chinese Academy of Sciences, Beijing 100029, China

Received 2 September 2005; accepted in revised form 14 December 2005

Abstract

Quaternary loess–soil sequences in China and Tajikistan are valuable archives of the chemical weathering history for arid and semi-arid regions of Asia. The development of new proxies independent of grain size are vital to reconstruct the long-term chemical weathering history of eolian deposits. In this study, we analyze major elemental and Rb, Sr, and Ba concentrations of decarbonated residue from representative loess and soil units along a north–south transect on the Chinese Loess Plateau and compare these concentrations among different grain-size fractions. Results show that most of the elemental abundances and ratios vary considerably among different grain-size fractions for both loess and paleosols, indicating transport-driven compositional differentiation of minerals during subaerial transport. However, $(CaO + Na_2O + MgO)/TiO_2$ ratios show little variation among different size fractions for the loess–soil transect. Loess–soil sequences at Lingtai (northern China) and Chashmanigar (southern Tajikistan) for the past 1.50–1.77 Ma show lower $(CaO + Na_2O + MgO)/TiO_2$ ratios in soil units than in adjacent loess horizons, in good agreement with greater weathering intensity in soils than in loess units. The $(CaO + Na_2O + MgO)/TiO_2$ ratio of the decarbonated residue is therefore a reliable proxy for chemical weathering of loess deposits that is independent of grain size. The $(CaO + Na_2O+MgO)/TiO_2$ ratios of the Lingtai and Chashmanigar sections display a relatively regular oscillation within a narrow range in the early Pleistocene, and a rapid increase in average values and in variance from 0.85–0.6 Ma to the present, indicating lowered chemical weathering intensity in both the dust source regions and the depositional areas. This event may be causally related to the expansion of northern hemisphere ice and/or the regional tectonic uplift of high mountains in Asia since the mid-Pleistocene.

1. Introduction

In Asia, arid environments dominate the middle latitudes, as in the Mu Us, Badain Jaran, Taklimakan, Karakum and Kyzylkum deserts (Fig. 1). These deserts, along with the adjoining loess regions, can be regarded as a single large, integrated arid and semi-arid region. The formation and evolution of this region is causally related to the rearrangement of the regional heat and moisture distributions, which may be attributed to the uplift of high mountains in Asia (Kutzbach et al., 1989; Ruddiman and Kutzbach, 1989; Manabe and Broccoli, 1990; Rea et al., 1998; An et al., 2001) and buildup of the northern hemisphere ice (Shackleton et al., 1984; Raymo, 1994). As such, chemical weathering intensity of superficial sediments in this region is highly sensitive to changes in regional heat and moisture balances.

Long-term chemical weathering history of these arid regions is hindered by the paucity of long, continuous, well-dated geological records. However, loess deposits downwind from the arid region are valuable archives of regional chemical weathering history. The loess sections in Asia with the greatest continuity, completeness and temporal range to date lie in China (Kukla, 1987; Liu, 1988; Kukla and An, 1989; Liu and Ding, 1998) and Tajikistan (Dodonov, 1991; Dodonov and Baiguzina, 1995; Shackleton et al., 1995; Ding et al., 2002a). The dust deposits on the Chinese Loess Plateau were transported by the East Asian winter monsoon (Liu, 1988; An et al., 1991;

* Corresponding author. Fax: +86 10 62032495.
E-mail address: yangsl@mail.iggcas.ac.cn (S. Yang).

0016-7037/$ - see front matter © 2005 Elsevier Inc. All rights reserved.
doi:10.1016/j.gca.2005.12.012

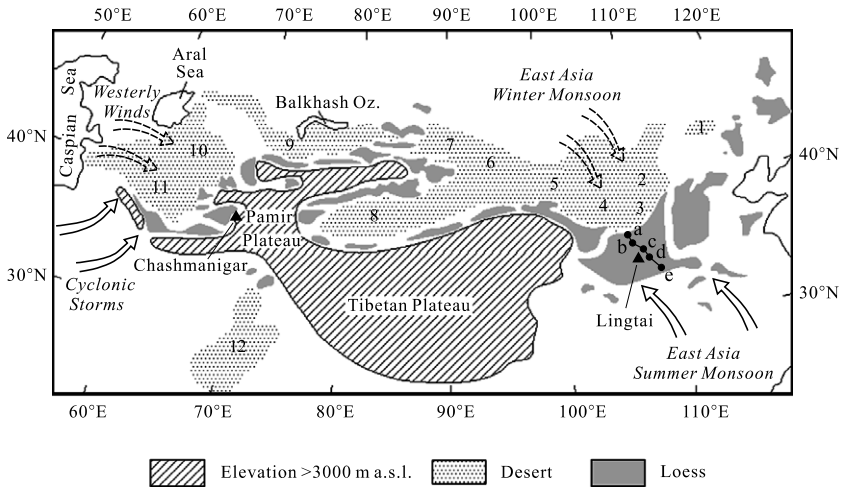

Fig. 1. Schematic map showing loess and desert distribution in Central Asia and China (modified from Dodonov, 1991). The solid and dashed arrows indicate the major moisture sources and dust transport winds, respectively, for the loess regions in Central Asia and northern China. Deserts: 1, Otindag; 2, Hobq; 3, Mu Us; 4, Tengger; 5, Badain Jaran; 6, Gobi; 7, Gurbantunggut (Junggar); 8, Taklimakan; 9, Muyunkum; 10, Kyzylkum; 11, Karakum; 12, Thar. Loess-soil transect: a, Jiyuan; b, Mubo; c, Ningxian; d, Binxian; e, Lantian.

Liu and Ding, 1998), while the regional westerly winds were responsible for the transport of loess in Central Asia (Lydolph, 1977; Ding et al., 2002a) (Fig. 1). At present, the East Asia monsoon system dominates the Chinese Loess Plateau, with hot, moist summers and cold, dry winters (Domrös and Peng, 1988). In contrast, the loess region of Tajikistan is characterized by hot, dry summers and mild, moist Mediterranean-type winters (Lydolph, 1977). Given that the loess deposits in the Chinese Loess Plateau and Central Asia are located at the eastern and western margins of the same large arid region, correlation of chemical weathering records between the far-separated regions would be useful for the understanding of the long-term hemispheric paleoclimate evolution and the history of regional tectonic uplift.

To date, elemental and isotopic ratios have been widely employed to quantify the chemical weathering intensity of loess deposits such as Ba/Sr (Gallet et al., 1996), Th/U (Gallet et al., 1996; Gu et al., 1997), Rb/Sr (Chen et al., 1999), Na/Al (Gu et al., 1999), Chemical Index of Alteration (CIA, see definition in Fig. 12) (Liu et al., 1995), Fe_2O_3(free)/Fe_2O_3(total) (Guo et al., 2000) and $^{87}Sr/^{86}Sr$ (Yang et al., 2001). Chemical weathering intensity reflected by these proxies is largely determined by three factors: chemical weathering in source regions, post-depositional weathering, and grain size. The third factor is related to depositional processes. Yang and Ding (2004) show that the grain size of loess is principally influenced by source-sink distance, i.e., the greater the transport distance the finer the grain size of dust deposits. Since elemental concentrations of dust deposits are partially dependent on grain-size changes (Wen, 1989; Eden et al., 1994), the elemental ratios of loess at different sites, which have undergone different transport distances, may be quite variable prior to any post-depositional weathering processes, even though they are transported and deposited by a single dust storm. Thus, a proxy free of grain-size effects must be developed to reconstruct long-term chemical weathering history of the region. In this study, we first develop such a proxy based on the investigation of elemental depletion characteristics in Chinese and Tajik loess and elemental ratios in different size fractions for a north–south transect on the Loess Plateau. Then we characterize the Pleistocene chemical weathering history recorded in loess deposits at Lingtai (northern China) and Chashmanigar (southern Tajikistan).

2. Site locations and lithostratigraphy

Our study transect runs north–south from Jiyuan near the Mu Us desert margin, to Lantian in the southernmost part of the Loess Plateau (Fig. 1). Five loess sections located at Jiyuan (37.14°N, 107.39°E), Mubo (36.43°N, 107.46°E), Ningxian (35.44°N, 107.94°E), Binxian (34.96°N, 108.05°E), and Lantian (34.15°N, 109.27°E) were studied (Fig. 1). At present, the mean annual temperature at Jiyuan is 7.9 °C and the annual precipitation 317 mm; the values for Lantian are 13 °C and ~600–650 mm. Both mean annual temperature and rainfall increase southwards along the loess transect. All loess sections consist of the loess(L)–soil(S) sequence S0, L1, and S1.

The Holocene soil S0 is dark in color because of its relatively high organic matter content. The upper part of the Holocene soil has been partly eroded or disturbed by agricultural activities at some sites along the transect. The loess unit L1 was deposited during the last glacial period and is yellowish in color and massive in structure. The L1 loess unit can be generally subdivided into five sub-units, termed L1-1, L1-2, L1-3, L1-4, and L1-5 (Fig. 2). L1-2 and L1-4 are weakly developed soils, and the others are typical loess horizons. Previous studies (Kukla, 1987; Kukla et al., 1988) have shown that L1-1 is correlated with ocean oxygen

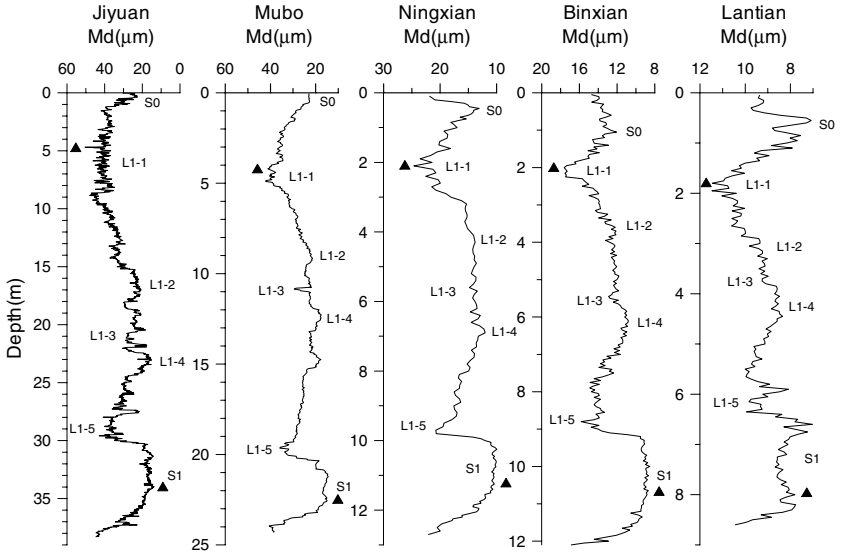

Fig. 2. Median grain-size (Md) records of the five sections along the north–south loess transect. Subdivision of the loess–soil sequences is designated. The stratigraphic positions for the selected samples in Figs. 10–12 are marked in solid triangles in each section. Note that the depth scale varies from one section to another. Grain-size data for Jiyuan and Lantian are from Ding et al. (1998) and Ding et al. (2005), respectively, and those for other three sections are from Yang and Ding (2004).

isotope stage 2, L1-5 with stage 4, and L1-2, L1-3, and L1-4 together with stage 3. The fivefold subdivision of L1 is clearly expressed in the grain-size variations (Fig. 2). The soil unit S1, being brownish or reddish in color and having an A-Bw-C or A-Bt-C horizon sequence, developed in the last interglacial period, marine oxygen isotope stage 5 (Kukla, 1987; Kukla et al., 1988). Grain size and thickness both decrease southward in loess and soil units, indicating strong spatial differentiation of dust during southward transport.

In addition to the transect sites, we studied two loess–soil sequences at Lingtai and Chashmanigar. The Lingtai section (35.0°N, 107.5°E) is situated in the central part of the Loess Plateau (Fig. 1), with mean annual temperature and precipitation values of 8.6 °C and 600 mm, respectively. The Lingtai loess has a thickness of 175 m, with each of the S0–L33 loess–soil units (Rutter et al., 1991) being readily identified in the field. Details of the stratigraphy and time scale of the section are given in Ding et al. (1999, 2002b). In this study, only the loess deposits above S20 are addressed (Fig. 3).

The Chashmanigar loess section (38.4°N, 69.8°E) is situated in southern Tajikistan where loess deposits are widely distributed on river terraces and piedmonts (Fig. 1). At present, the mean annual temperature and precipitation at Chashmanigar are about 11 °C and 842 mm. The Chashmanigar section, with a thickness of ~205 m, is underlain by gravel. The lowermost part of the section is covered by slumps, only the upper 195 m being accessible for study. According to Ding et al. (2002a), a total of 29 paleosols have been identified in the section, which can be correlated with the S0-S24 portion of the Chinese loess (Fig. 4). Paleomagnetic dating (Ding et al., 2002a) suggests a basal age of about 1.77 Ma for the Chashmanigar loess

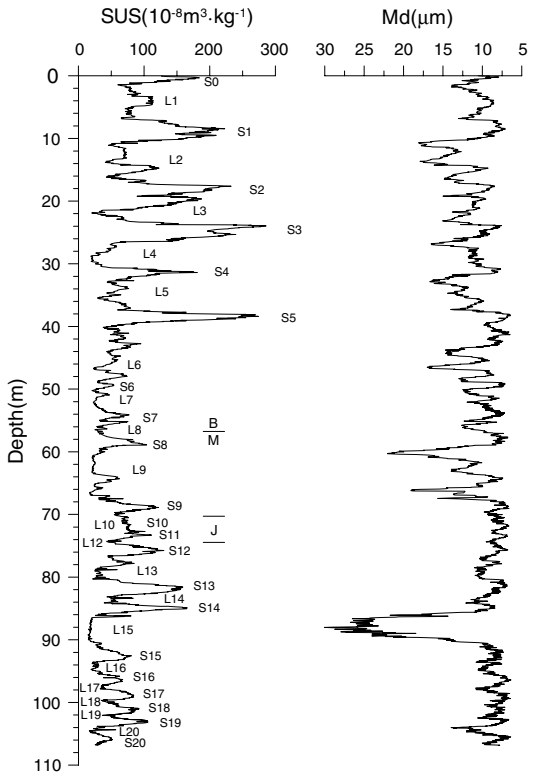

Fig. 3. Magnetic susceptibility (SUS) and median grain-size (Md) records of the loess–soil sequence at Lingtai, the Chinese Loess Plateau (after Yang and Ding, 2004). The major paleomagnetic reversal is indicated (modified from Yang and Ding, 2004). Most of the soil units (S*i*) and major loess beds (L*i*) are indicated.

(Fig. 4). Details of the stratigraphy and time scale of the section are given in Ding et al. (2002a).

In general, the stratigraphic structure of the Lingtai and Chashmanigar sections can be divided into two parts.

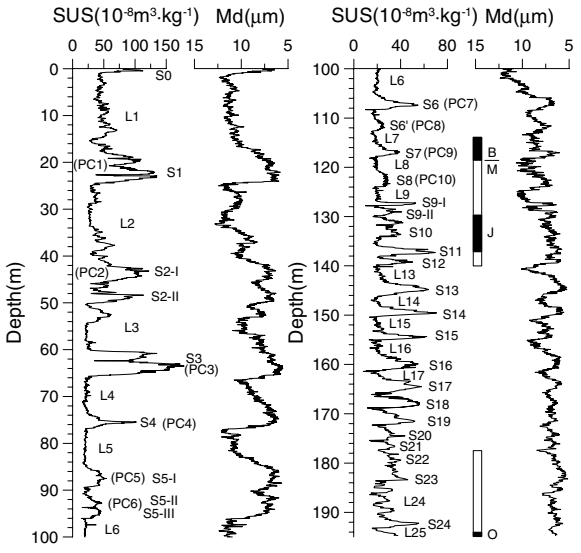

Fig. 4. Magnetic susceptibility (SUS) and median grain-size (Md) records of the Chashmanigar loess section, southern Tajikistan, together with paleomagnetic analytical results (adapted from Ding et al., 2002a). The loess–soil units are labeled using both the L*i*–S*i* system, as used in studies of Chinese loess, and the PC*i* system traditionally used in Tajikistan.

The upper parts (above S8) have a thickness of 124 and 59 m, and the lower parts 71 and 48 m for Chashmanigar and Lingtai, respectively (Figs. 3 and 4). The paleosols in the lower parts are relatively thin and closely spaced, while upper-section paleosols are much thicker and separated by thicker loess layers. Throughout section, paleosols are characterized consistently by higher susceptibility values and finer particle sizes, compared to the loess horizons above and below them (Figs. 2–4). The alternation of loess and soils documents large-scale oscillations between glacial and interglacial conditions during the Pleistocene (Kukla, 1987; Liu, 1988).

3. Sampling and analytical procedures

For the loess–soil transect, two samples were selected from each section, one from the last glacial maximum loess unit (L1-1), and the other from the last interglacial soil unit (S1). The basis of this sample selection was the median grain-size record shown in Fig. 2. For loess horizon L1-1, samples were selected from units containing the coarsest grain sizes, whereas samples from soil unit S1 were generally taken from the finest grain-size units (marked in Fig. 2). At Lingtai, 494 samples were taken at vertical intervals of ~20–50 cm, and 842 samples were taken at vertical intervals of ~20–40 cm at Chashmanigar. According to the time scales of the two sections (Ding et al., 2002a,b), this sample spacing yields a mean depositional resolution of ~3000 years for the Lingtai section and of ~2000 years for the Chashmanigar section.

The samples from the north–south transect were divided into six size fractions (<2, 2–5, 5–16, 16–32, 32–63, and >63μm) using the pipette method. These samples, together with those from Lingtai and Chashmanigar, were first finely ground in agate mortar. Then they were treated with 1 M acetic acid for over 12 h at room temperature to remove carbonate. The residue was rinsed, dried up in an oven at 105 °C. For X-ray fluorescence analysis, 1.2 g of the sample powder was mixed with 6 g of dry lithium tetraborate ($Li_2B_4O_7$) and fused to glass beads in Pt crucibles. Major element and Rb, Sr, and Ba abundances were then determined using the Shimadzu XRF-1500 spectrometer in the Institute of Geology and Geophysics, CAS. Analytical uncertainties are ±5% for all major elements except for MnO and P_2O_5 (up to ±10%), ±6% for Ba and Sr, and ±10% for Rb. Loss on ignition (LOI) was obtained by weighing after 1 h of calcination at 950 °C.

4. Characteristics of elemental depletions in loess deposits

4.1. Major element and Rb, Sr, and Ba abundances of the Lingtai and Chashmanigar sections

The geochemical data of the carbonate-free samples from Lingtai and Chashmanigar are presented in electronic annexes EA-1 and EA-2, respectively. In comparison to the Tajik loess, the Chinese loess is characterized by higher SiO_2 concentrations (70–75 wt% vs. 66–71 wt%), and by lower concentrations of Fe_2O_3 (4.4–5.6 wt% vs. 5.4–6.8 wt%), Al_2O_3 (13.0–15.5 wt% vs. 14.5–16.6 wt%), MgO (1.2–2.2 wt% vs. 2.0–3.2 wt%) and CaO (0.6–2.0 wt% vs. 0.7–4.0 wt%) (Figs. 5 and 6). From 1.5 Ma to the present, the Fe_2O_3 content increases gradually at Lingtai, while the contents of MgO, CaO, and Na_2O show a gradual increase since ~0.6 Ma (Fig. 5). For the Chashmanigar section, there is an upward decrease in K_2O and an accompanying increase in Na_2O since 1.77 Ma (Fig. 6). The Al_2O_3 concentrations at Chashmanigar exhibit stepwise decreases at ~1.3, ~0.9, and ~0.5 Ma, while MgO, CaO, and Fe_2O_3 increase markedly since 0.4–0.5 Ma. Rb, Sr, and Ba values are comparable between Lingtai and Chashmanigar. In the Lingtai section, most paleosols exhibit higher SiO_2 and Rb, and lower P_2O_5 concentrations than adjacent loess units, while only some paleosols at Chashmanigar show such characteristics. In both sections, paleosols are generally characterized by higher concentrations of TiO_2, Al_2O_3, MnO, K_2O, and Ba, and lower concentrations of CaO, MgO, Na_2O, and Sr, compared to the loess horizons above and below them.

4.2. Changes in major element concentrations during pedogenesis

Chemical weathering leads to the removal of more soluble components (Loughnan, 1969). In a plot of Na_2O/Al_2O_3 vs. K_2O/Al_2O_3 introduced by Garrels and Mackenzie (1971), depletion of Na and K is evident in all loess and paleosol samples for both sections, compared to average upper continental crust (UCC) (Taylor and McLennan, 1985) (Fig. 7). Moreover, all the loess and soil samples exhibit much more Na depletion than K depletion, and

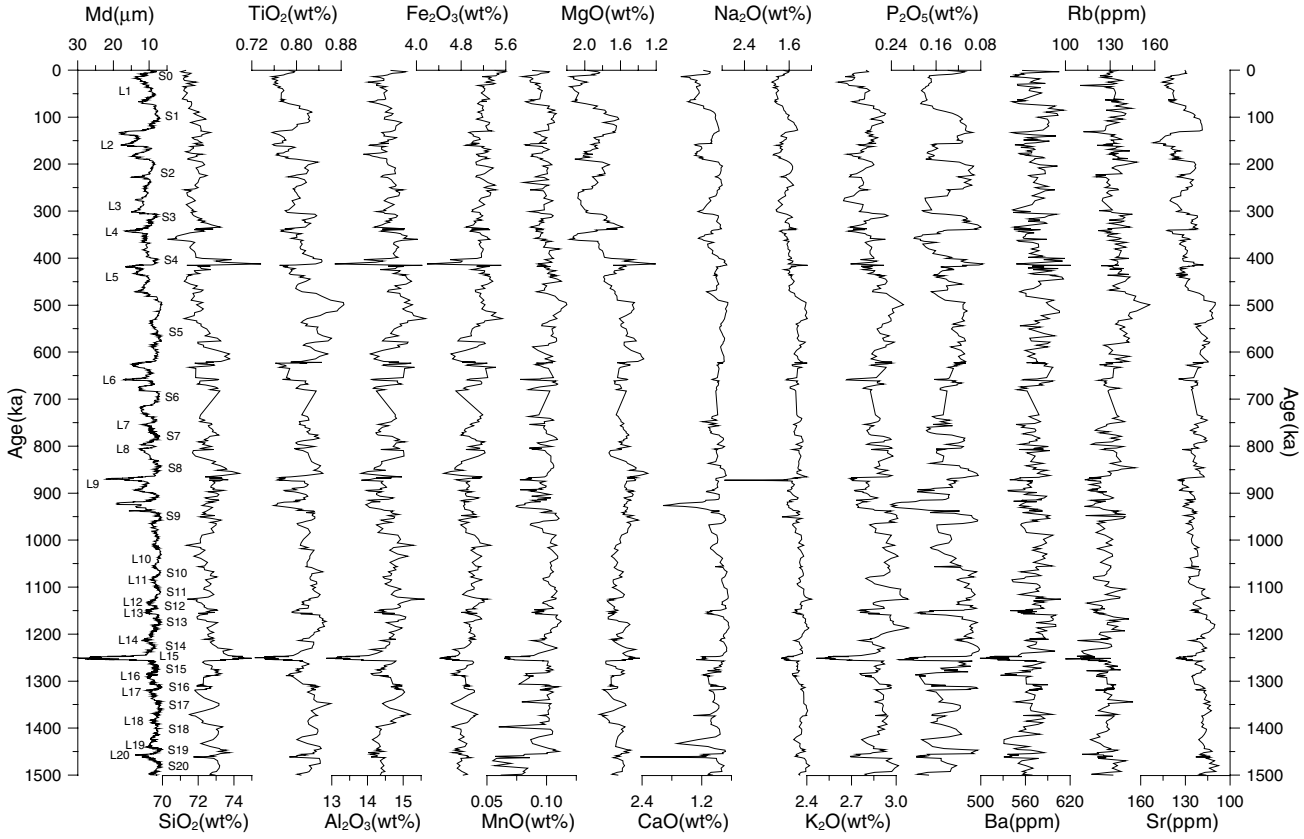

Fig. 5. Major element and Ba, Rb, and Sr abundances of loess–soil sequence at Lingtai. The major and trace element data are recalculated on a volatile-free basis. The time scale is taken from Ding et al. (2002b).

the paleosols show slightly more Na depletion than loess samples. The Chashmanigar section has a larger spread in K_2O/Al_2O_3 ratios than the Lingtai section, which can be explained by larger variations in K_2O contents (2.5–3.5 wt%) at Chashmanigar (Fig. 6) compared to Lingtai (2.5–3.0 wt%) (Fig. 5). These changes in K_2O concentrations may be related to variations in the amount of K-rich minerals (e.g., mica) present.

The depletion of Na and K in both loess and paleosol samples indicates that loess materials have been subjected to considerable weathering processes before transport, consistent with previous studies (Gallet et al., 1998; Ding et al., 2001a; Jahn et al., 2001). Therefore, it is hard to estimate a real gain/loss in elemental abundances within the loess deposits. However, the relative changes in elemental abundances between paleosols and loess units can still be estimated using the method of Gallet et al. (1996). A basic assumption with this method is that the initial composition of a particular paleosol layer was the same as that of the underlying loess. For example, L2 loess layer is the "parent loess" of S1 soil unit. This makes it possible to quantitatively examine the change in elemental abundances due to pedogenesis, a precondition for the development of weathering proxies. We then performed a constant oxide calculation (Garrels and Mackenzie, 1971) for the soil units in the two sections, using TiO_2 as the constant oxide (Figs. 8 and 9). In both sections, the SiO_2 shows a small loss (<8%), and a small gain or loss (<10%) for Al_2O_3, Fe_2O_3, and K_2O. Most paleosols of the two sections are characterized by a major loss of P_2O_5 (up to 55%), CaO (up to 40%), Na_2O (up to 25%), and MgO (up to 25%), and gain of MnO (up to 33%). The gain–loss patterns of the two sections are essentially similar to those calculated using Al_2O_3 as the constant oxide (not shown). These results are consistent with previous studies of Chinese loess weathering (Gallet et al., 1996; Jahn et al., 2001).

5. Major element and Rb, Sr, and Ba characteristics in different size fractions for the loess transect

5.1. Elemental abundances and ratios

Results from our transect study sites (given in electronic annex EA-3) show that SiO_2, CaO, Na_2O, and Sr concentrations are higher in coarser fractions, while Al_2O_3, Fe_2O_3, MnO, MgO, K_2O, P_2O_5, Ba, and Rb concentrations are higher in finer fractions, for both loess and paleosols (Figs. 10 and 11). TiO_2 content shows little variation among different fractions except for slightly higher values in size fractions 2–5 and 5–16 μm.

The values of the weathering proxies used in loess studies, such as CIA, Na_2O/Al_2O_3, Rb/Sr, and Ba/Sr, are calculated for different size fractions (Fig. 12). Again, those proxies vary considerably with grain-size changes.

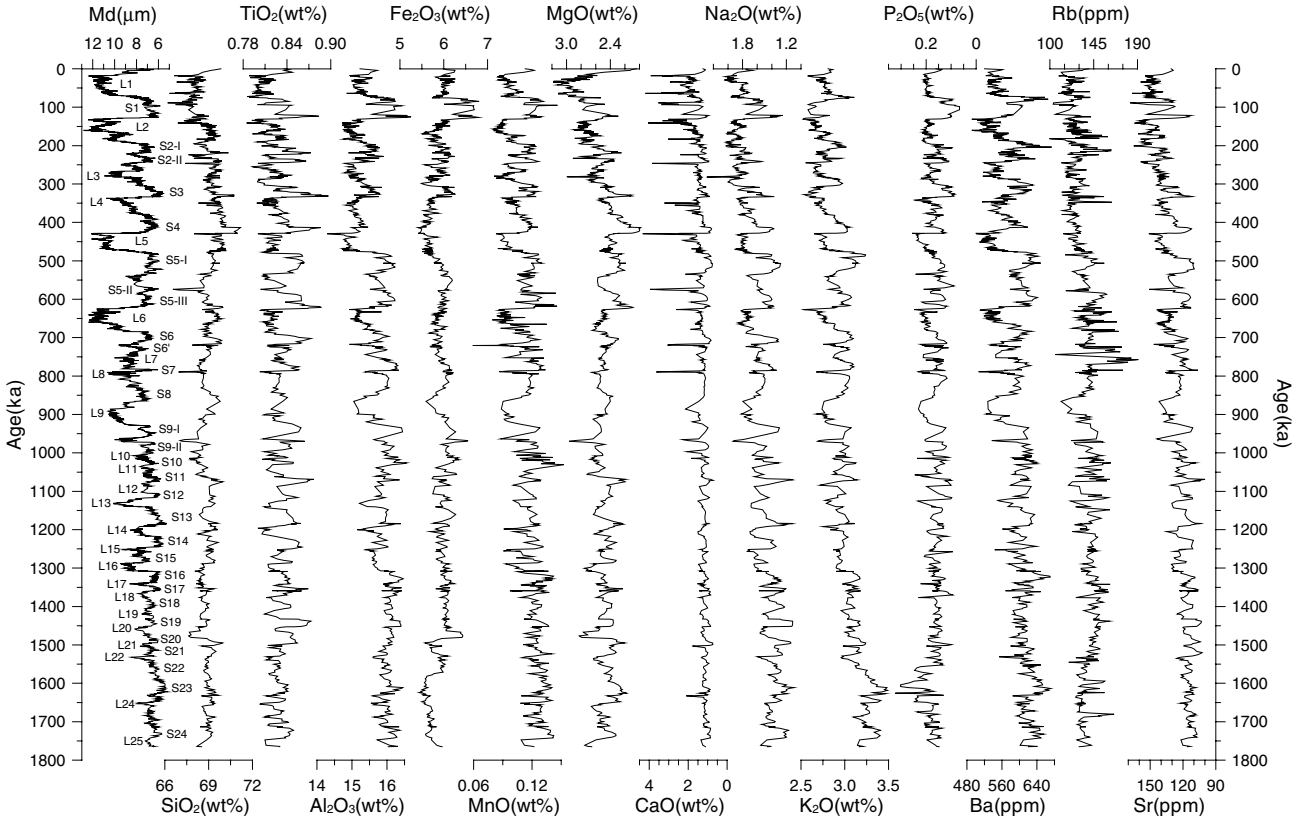

Fig. 6. Major element and Ba, Rb, and Sr abundances of loess–soil sequence at Chashmanigar. The major and trace element data are recalculated on a volatile-free basis. The time scale is taken from Ding et al. (2002a).

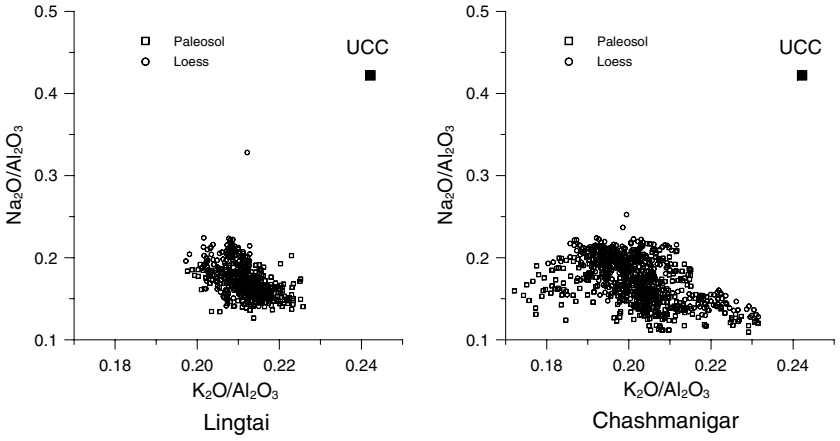

Fig. 7. Diagrams showing variations in Na_2O/Al_2O_3 (molar ratio) vs. K_2O/Al_2O_3 (molar ratio) for all the loess and soil samples from Lingtai and Chashmanigar. The UCC values (Taylor and McLennan, 1985) are shown for comparison.

From clay (<2 μm) to sand fraction (>63 μm), CIA values decrease from ~75–80 to ~55, and Na_2O/Al_2O_3 ratios increase from ~0.03 to ~0.32–0.37, while Rb/Sr and Ba/Sr ratios decrease from ~1.3–2.0 to ~0.5 and from ~6–11 to ~3, respectively. In general, the spatial (north–south) changes in elemental abundances and ratios in a specific size fraction are minor for both glacial loess and interglacial soil units when compared to variations among different size fractions. For a specific section, the temporal changes (between loess and soil units) in elemental abundances and ratios in a specific size fraction are also minor when compared among different size fractions.

5.2. The relationship between elemental differentiation and mineralogical constituent among different grain-size fractions

The variations in elemental ratios in our loess study can be understood in terms of mineralogic changes

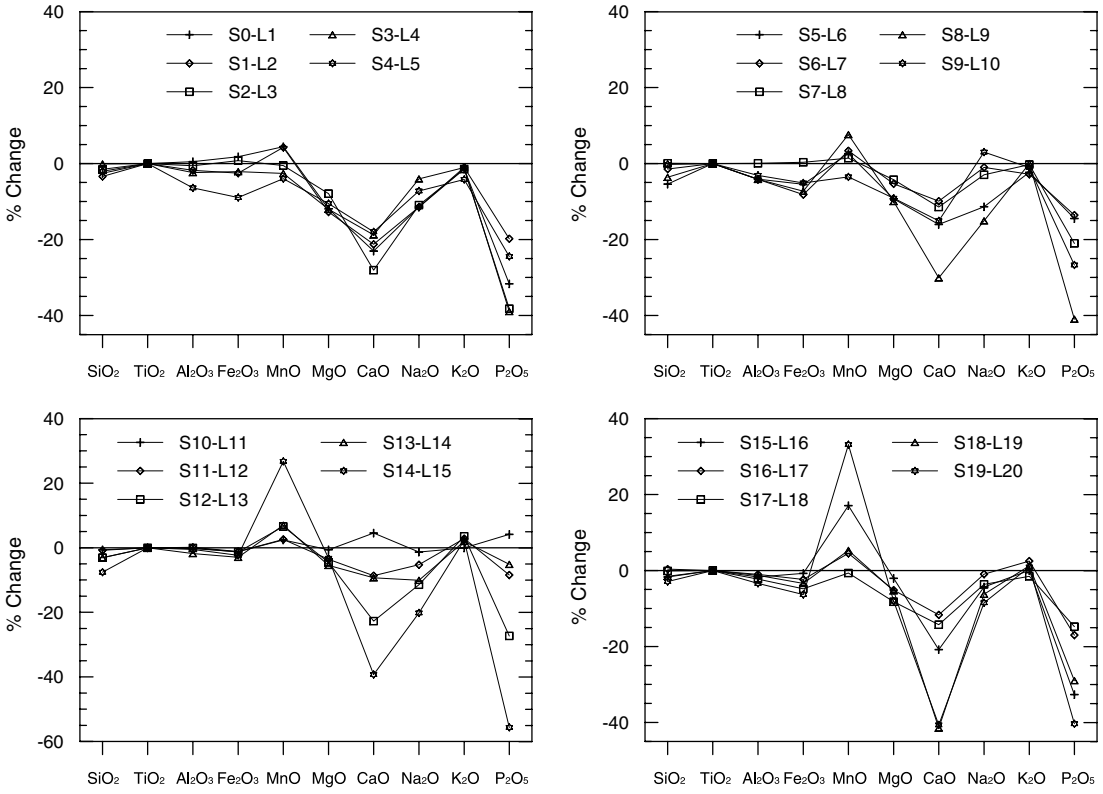

Fig. 8. Results of constant oxide (TiO_2) calculations for the Lingtai section. The contents of major element oxides were first averaged for each loess and soil unit, then followed by the procedure: (1) calculate the gain–loss factor $w = TiO_{2(loess)}/TiO_{2(soil)}$, (2) calculate the "true" gain or loss for each oxide $r(\%) = [(w \times Oxide_{(soil)} - Oxide_{(loess)})/Oxide_{(loess)}] \times 100$.

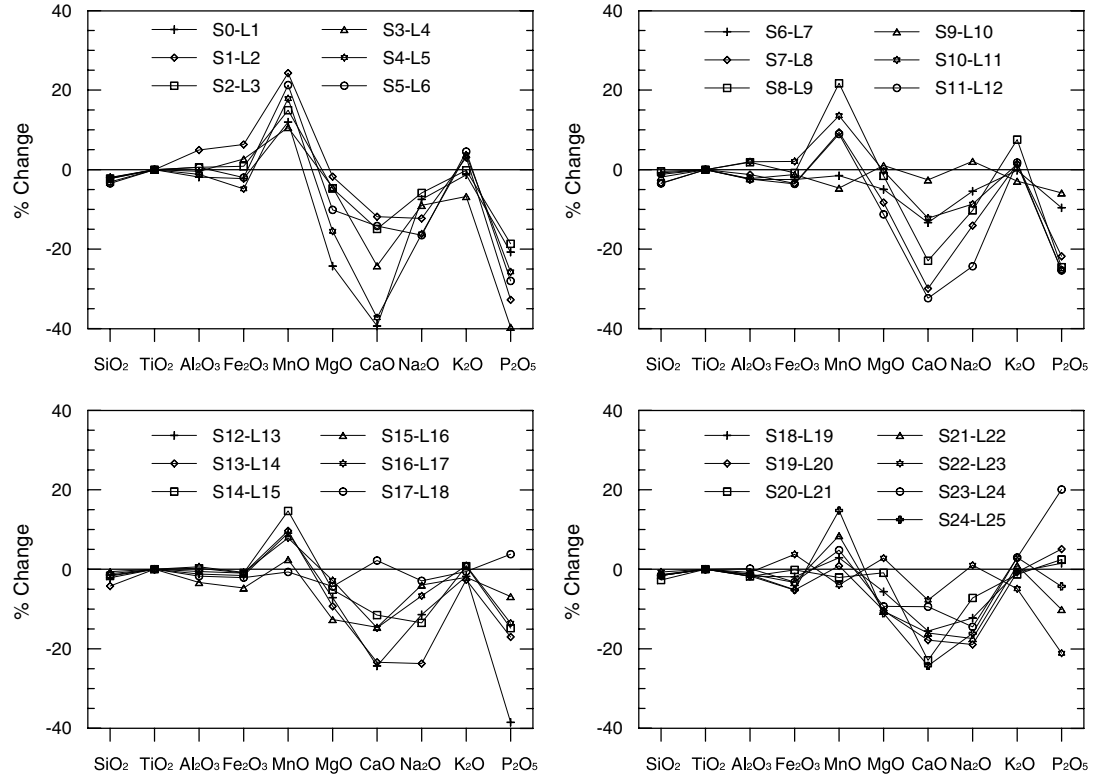

Fig. 9. Results of constant oxide (TiO_2) calculations for the Chashmanigar section. The calculation method is the same as in Fig. 8.

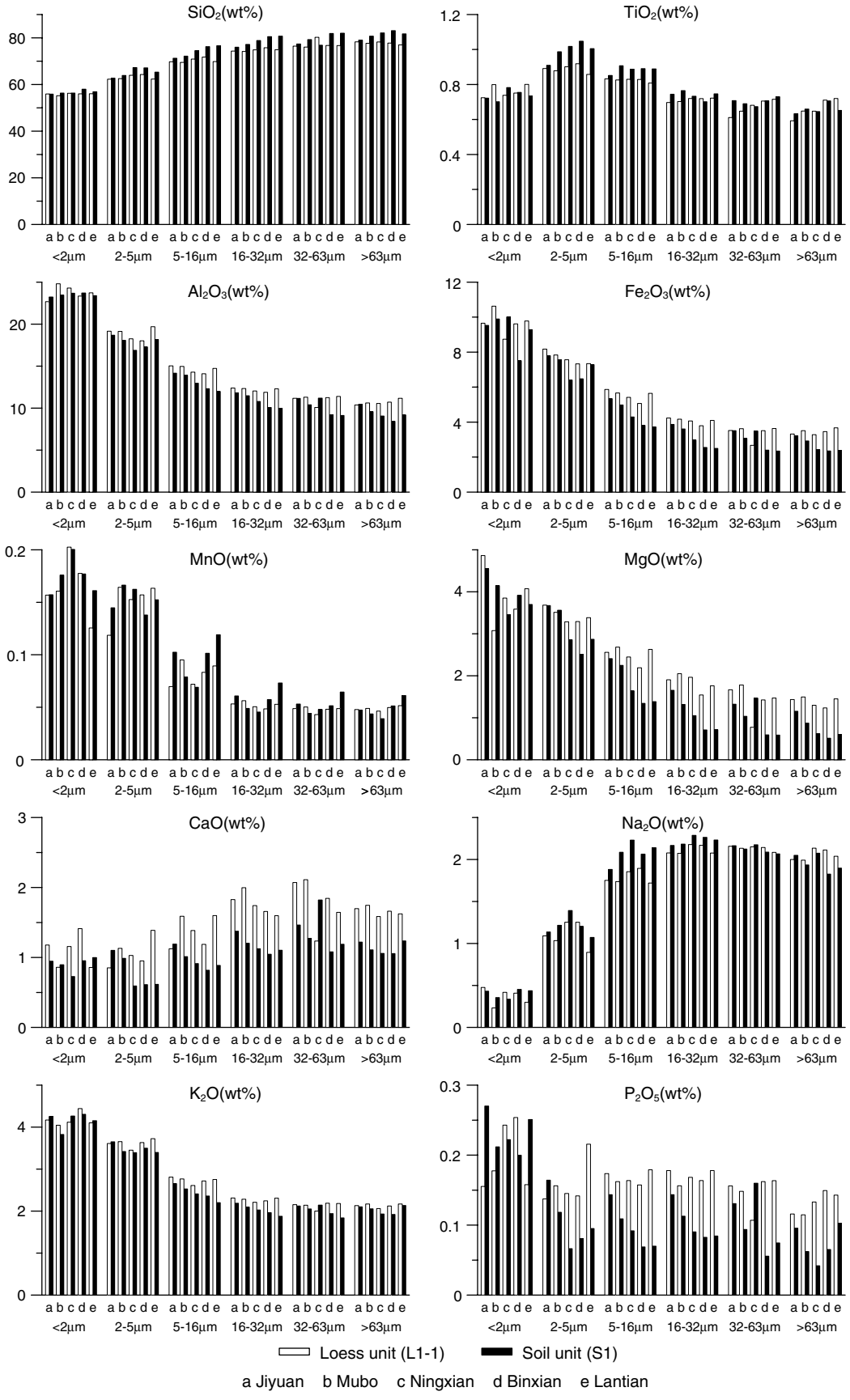

Fig. 10. Major element concentrations (recalculated on a volatile-free basis) in different grain-size fractions for the north–south loess transect on the Chinese Loess Plateau.

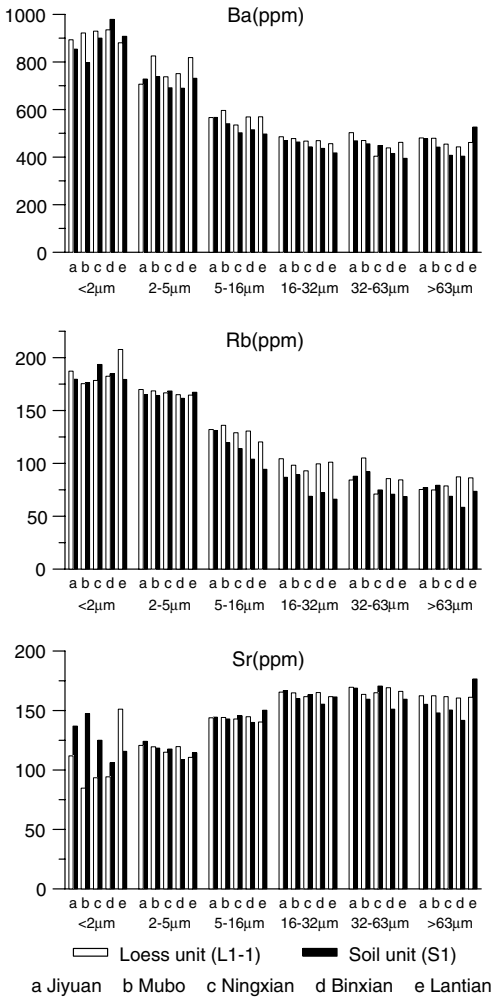

Fig. 11. Ba, Rb, and Sr abundances (recalculated on a volatile-free basis) in different grain-size fractions for the north–south loess transect on the Chinese Loess Plateau.

among different grain-size fractions identified by previous studies (Liu, 1988; Eden et al., 1994). Loess is a highly homogeneous mixture of atmospheric dust composed of minerals of several origins (Liu, 1988). In the silt-sized fraction of loess, the most abundant minerals are quartz, feldspar, and mica (Liu, 1988; Eden et al., 1994). According to Eden et al. (1994), quartz and feldspar contents decrease from coarse to fine fractions, while mica and chlorite increase. This is corroborated by our results (Fig. 10). The SiO_2, Al_2O_3, and K_2O variations are consistent with the increased quartz and decreased mica in coarse fractions. Higher CaO and Na_2O in coarse fractions suggest increased plagioclase. Fe_2O_3 variations indicate the increased iron oxides in fine fractions, while higher MgO in fine fractions may be related to the increased chlorite. In addition, the abundant clay minerals (e.g., illite, kaolinite, and chlorite) in the clay-sized fraction (<2 μm) (Liu, 1988; Eden et al., 1994), mainly of detrital origin (Liu, 1988; Ji et al., 1999), are also responsible for the highest peaks of Al_2O_3, Fe_2O_3, MgO, and K_2O in that fraction.

In loess deposits, TiO_2 mainly comes from Ti-rich minerals (e.g., rutile, anatase, brookite, and sphene) (Liu, 1988). These minerals are common in clastic sediments in the dust source regions as part of the heavy mineral fraction. The invariance of TiO_2 with grain size indicates that the Ti-rich minerals may be relatively evenly distributed in different size fractions, which possibly suggests unique behaviors of Ti-rich minerals to wind transport and sorting. However, this interpretation requires more evidence and mineralogical analyses.

6. A new proxy for chemical weathering intensity

The ratio of mobile to immobile elements is always adopted as a good measure of the degree of weathering (Nesbitt and Young, 1982; Gallet et al., 1996; Chen et al., 1999; Gu et al., 1999; Ding et al., 2001a; Jahn et al., 2001; Muhs et al., 2001). As shown in Figs. 8 and 9, P, Ca, Na, and Mg are the most mobile elements in loess deposits, while Ti, Al, Si, and Fe are the least mobile. Because silicate minerals are the major constituent of loess material and P mainly occurs in the accessory minerals such as apatite and monazite, we assume that the sum of CaO, Na_2O, and MgO contents reflects the general depletions of elements from loess during weathering processes. The $(CaO + Na_2O + MgO)/SiO_2$ ratios are higher in finer size fractions, while the $(CaO + Na_2O + MgO)/Al_2O_3$ and $(CaO + Na_2O + MgO)/Fe_2O_3$ values are higher in the coarser fractions (Fig. 12). However, it is highly significant that $(CaO + Na_2O + MgO)/TiO_2$ values show small variations among the six size fractions (Fig. 12).

Most elemental contents (Figs. 10 and 11) and ratios (Fig. 12) vary with changes in grain size, indicating that elemental distribution is dependent on grain size to a considerable extent. The new proxy $(CaO + Na_2O + MgO)/TiO_2$ suffers little grain-size influence, which can be explained by two mechanisms. First, TiO_2 contents show small variations among different size fractions (Fig. 10). Second, the higher MgO contents in fine size fractions is offset by lower Na_2O and CaO (Fig. 10), so the sum of Ca, Mg, and Na varies little with grain-size changes (Fig. 12). Therefore, $(CaO + Na_2O + MgO)/TiO_2$ of decarbonated residue may be regarded as the best proxy for chemical weathering intensity of loess deposits.

In Chinese loess, carbonate content is up to 20% in loess horizons, while it is near zero in paleosols (Liu, 1988; Ding et al., 2001b). Therefore, the $(CaO + Na_2O + MgO)/TiO_2$ values would be higher for loess horizons and would change little for soil units if bulk sample chemistry was considered. We arrive at maximum estimates of chemical weathering for the loess units by measuring the $(CaO + Na_2O + MgO)/TiO_2$ ratio of the decarbonated residue because carbonate, the most readily weathered component in dust deposits, remains to be leached out of loess units.

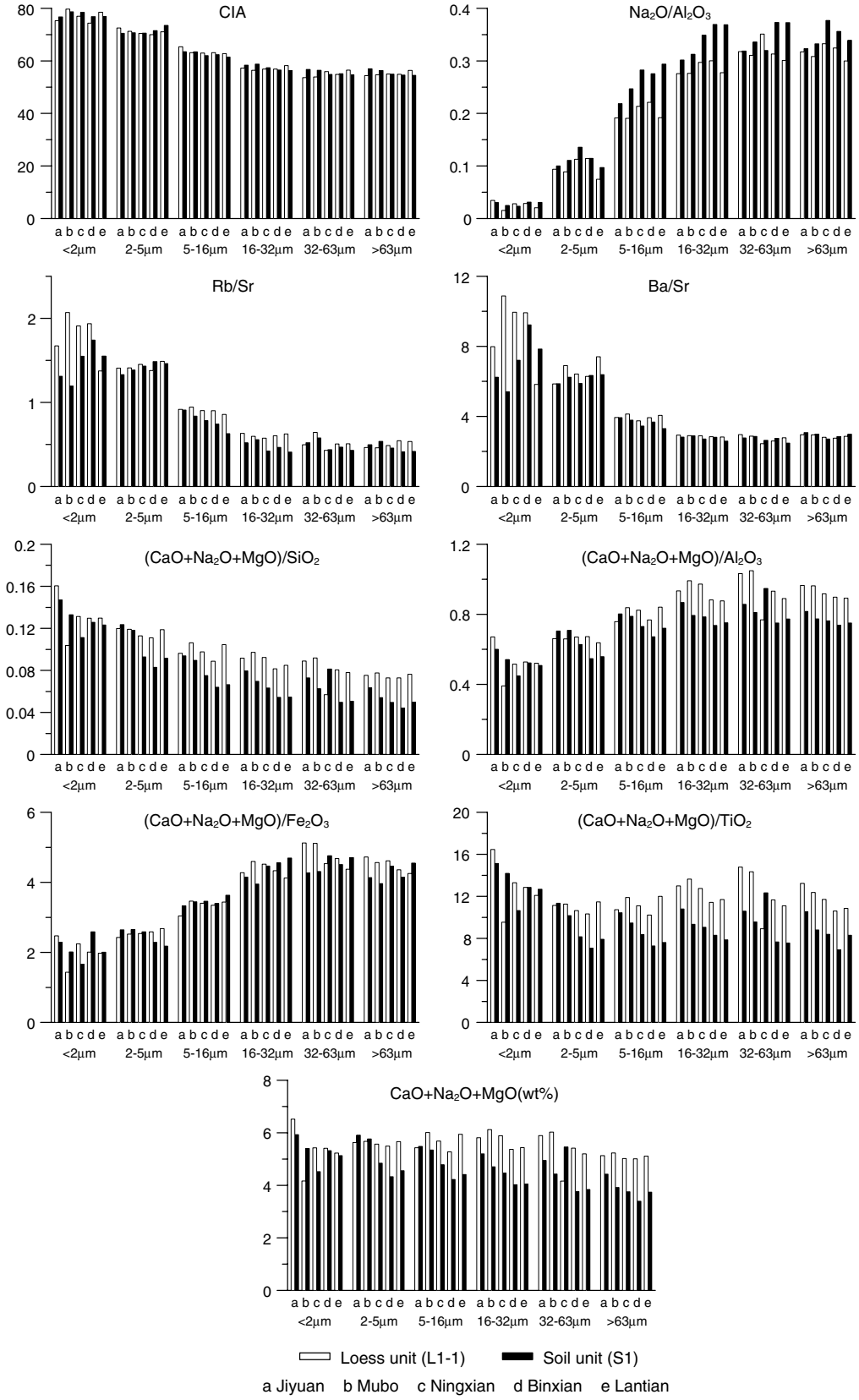

Fig. 12. Various elemental ratios (molar ratios except Rb/Sr and Ba/Sr) and the sum of CaO, MgO, and Na_2O contents in different grain-size fractions for the north–south loess transect on the Chinese Loess Plateau. CIA = $[Al_2O_3/(Al_2O_3 + CaO^* + Na_2O + K_2O)] \times 100$ (molar ratio), where CaO* is the amount of CaO incorporated in the silicate fraction of the rock. This proxy was first proposed by Nesbitt and Young (1982) and introduced in loess studies by Liu et al. (1995).

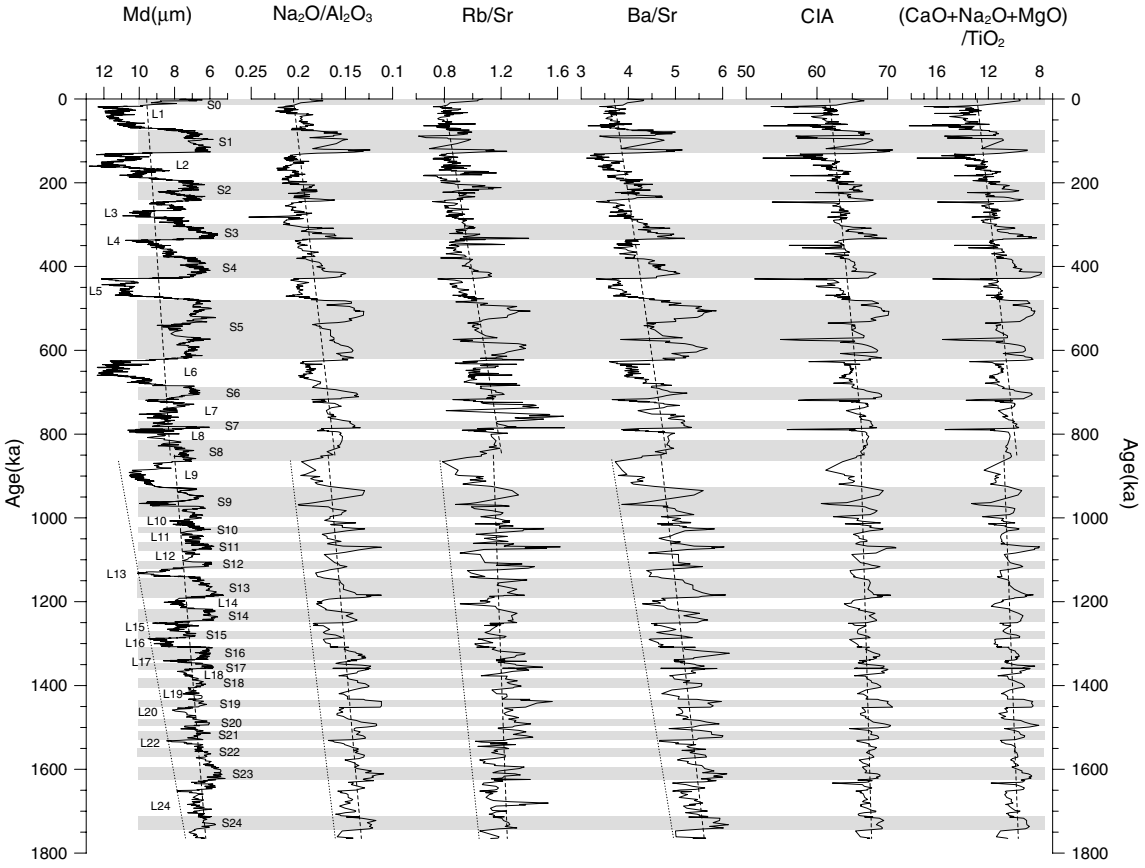

Fig. 13. Changes in median grain size (Md), Na_2O/Al_2O_3 (molar ratio), Rb/Sr, Ba/Sr, CIA, and $(CaO + Na_2O + MgO)/TiO_2$ (molar ratio) at Chashmanigar. The time scale is taken from Ding et al. (2002a). The dashed lines are linear fits of each curve for different time intervals. The shaded zones indicate interglacials. Note the gradual increase or decrease of the median grain size, Na_2O/Al_2O_3, Rb/Sr, and Ba/Sr for the loess units from 1.77 to 0.85 Ma, indicated by the dotted lines.

7. Pleistocene chemical weathering history recorded in loess deposits of China and Tajikistan

7.1. Comparison of elemental ratio records

The alternation of loess and soils in the Chashmanigar and Lingtai sections is clearly expressed in the elemental ratio curves (Figs. 13 and 14), with soils exhibiting lower Na_2O/Al_2O_3 and $(CaO + Na_2O + MgO)/TiO_2$ values and higher Rb/Sr, Ba/Sr, and CIA values compared to the adjacent loess units. In the Chashmanigar section, the median grain size increases progressively from 1.77 to 0.85 Ma, especially in the case of the loess units (Fig. 13). Likewise, the Na_2O/Al_2O_3, Rb/Sr, and Ba/Sr values display an oscillatory increase or decrease over the same time interval, similar to the grain-size record. However, CIA and $(CaO + Na_2O + MgO)/TiO_2$ show relatively regular fluctuations during the time interval 1.77–0.85 Ma, indicating that the variation patterns of Na_2O/Al_2O_3, Rb/Sr, and Ba/Sr in this time interval may be influenced by the grain size. From 0.85 Ma to the present, the Na_2O/Al_2O_3 and $(CaO + Na_2O + MgO)/TiO_2$ values increase gradually, while Rb/Sr, Ba/Sr, and CIA decrease.

In the Lingtai section, the elemental ratio curves can also be divided into two parts (Fig. 14). From 1.5 to 0.6 Ma, the five elemental ratio proxies generally show regular fluctuations. From 0.6 Ma to the present, Na_2O/Al_2O_3 show a gradual increase; Rb/Sr and Ba/Sr display a gradual decrease; and CIA and $(CaO + Na_2O + MgO)/TiO_2$ show a rapid decrease and increase, respectively. The difference between the new proxy and other elemental ratios lies in the fact that the $(CaO + Na_2O + MgO)/TiO_2$ curve is much smoother, and some soil units (e.g., S4 and S8), which are not well expressed in the other four elemental ratio curves, are clearly seen in the the $(CaO + Na_2O + MgO)/TiO_2$ record.

7.2. Pleistocene chemical weathering history

The comparison of the new proxy with other elemental ratios at Lingtai and Chashmanigar further suggests that $(CaO + Na_2O + MgO)/TiO_2$ does eliminate the grain-size effects to a large extent and is a robust proxy for chemical weathering intensity. It also appears that CIA is less influenced by grain size than is Na_2O/Al_2O_3, Rb/Sr, and Ba/Sr. This may be related to the fact that CIA incorporates the

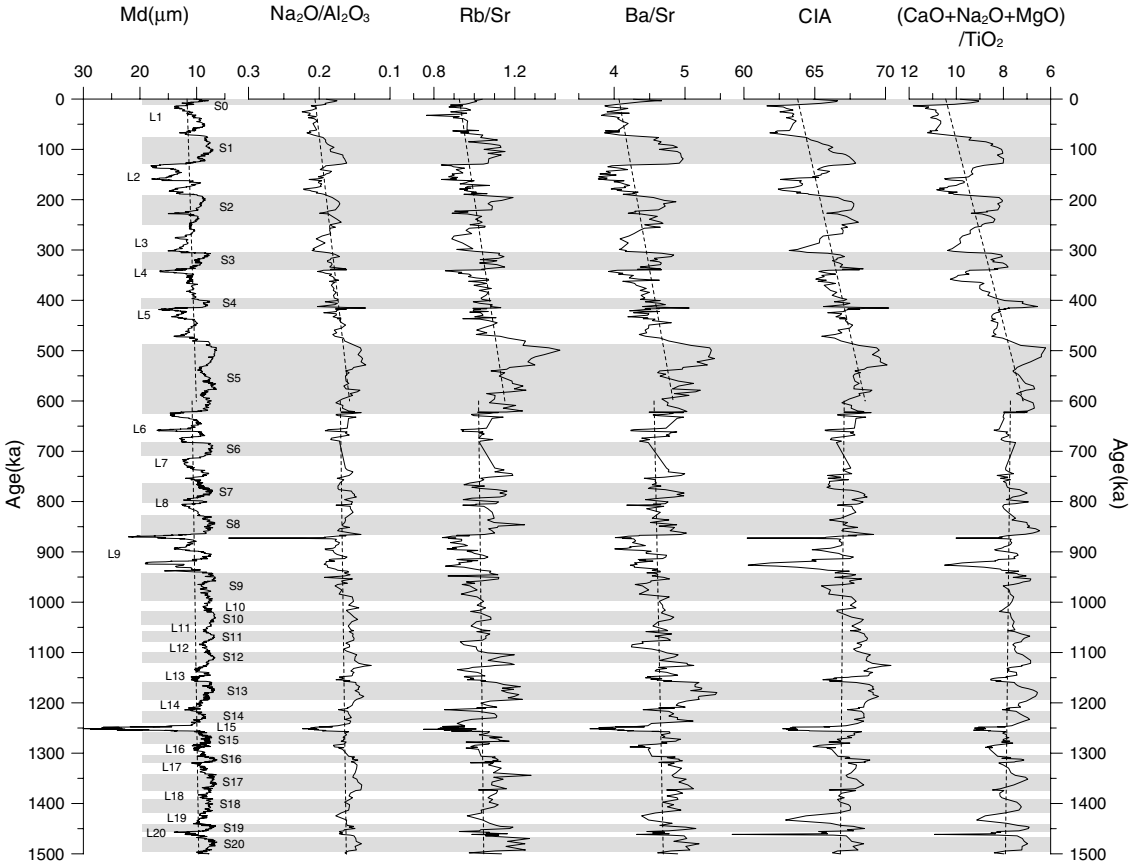

Fig. 14. Changes in median grain size (Md), Na_2O/Al_2O_3 (molar ratio), Rb/Sr, Ba/Sr, CIA, and $(CaO + Na_2O + MgO)/TiO_2$ (molar ratio) at Lingtai. The time scale is taken from Ding et al. (2002b). The dashed lines are linear fits of each curve for different time intervals. The shaded zones indicate interglacials.

loss of Ca, Na, and K, rather than a single element, into its calculation (Nesbitt and Young, 1982). As seen in Fig. 10, the contents of Na_2O and CaO are higher in coarser fractions, while K_2O content is higher in finer fractions. Thus the sum of Ca, Na, and K may offset grain-size effects to some extent. In the Lingtai and Chashmanigar sections, the CIA and $(CaO + Na_2O + MgO)/TiO_2$ variations are quite similar through time. This may result from (1) CIA being partially independent of grain size, and (2) a small difference in median grain size (generally <10 μm) between loess and soil units in the two sections. In this context, the TiO_2 based new proxy will reflect chemical weathering intensity more reliably in dust deposits with large grain-size variations, which are distributed in the areas close to dust source regions (Yang and Ding, 2004; Ding et al., 2005).

At Chashmanigar, the $(CaO + Na_2O + MgO)/TiO_2$ values show a stable oscillation between 8 and 13 from 1.77 to 0.85 Ma (Fig. 15). From 0.85 Ma to the present, the proxy increases from 10 to 13, as indicated by the fit line (Fig. 15). At Lingtai, the $(CaO + Na_2O + MgO)/TiO_2$ ratio also displays a relatively stable oscillation between 6.5 and 9.5 from 1.5 to 0.6 Ma except for the loess units L9 and L20, and a rapid increase from 7.2 to 10.5 for the past 0.6 Ma (see the fit line) (Fig. 15).

In both sections, glacial loess units display consistently higher $(CaO + Na_2O + MgO)/TiO_2$ values compared to the adjacent interglacial soil horizons, indicating lower chemical weathering intensity for loess units. The weathering intensity shows a rapid decrease since 0.85 Ma for the Tajik loess and since 0.6 Ma for the Chinese loess. Both sections are characterized by high frequency, small amplitude oscillations for the early Pleistocene and low frequency, large amplitude oscillations after the mid-Pleistocene (Fig. 15).

8. Discussion

Loess in Tajikistan was transported by regional westerly winds from Karakum and Kyzylkum deserts (Lydolph, 1977; Ding et al., 2002a), while the Chinese loess was transported by East Asian winter monsoon from the arid regions in northwestern China (Liu and Ding, 1998; Sun, 2002) (Fig. 1). The $(CaO + Na_2O + MgO)/TiO_2$ ratios of both the Lingtai and Chashmanigar loess–soil sequences indicate that the chemical weathering intensity of loess has decreased rapidly since 0.85–0.6 Ma. This implies that the weathering intensity of the large arid and semi-arid region decreased since the mid-Pleistocene, as the

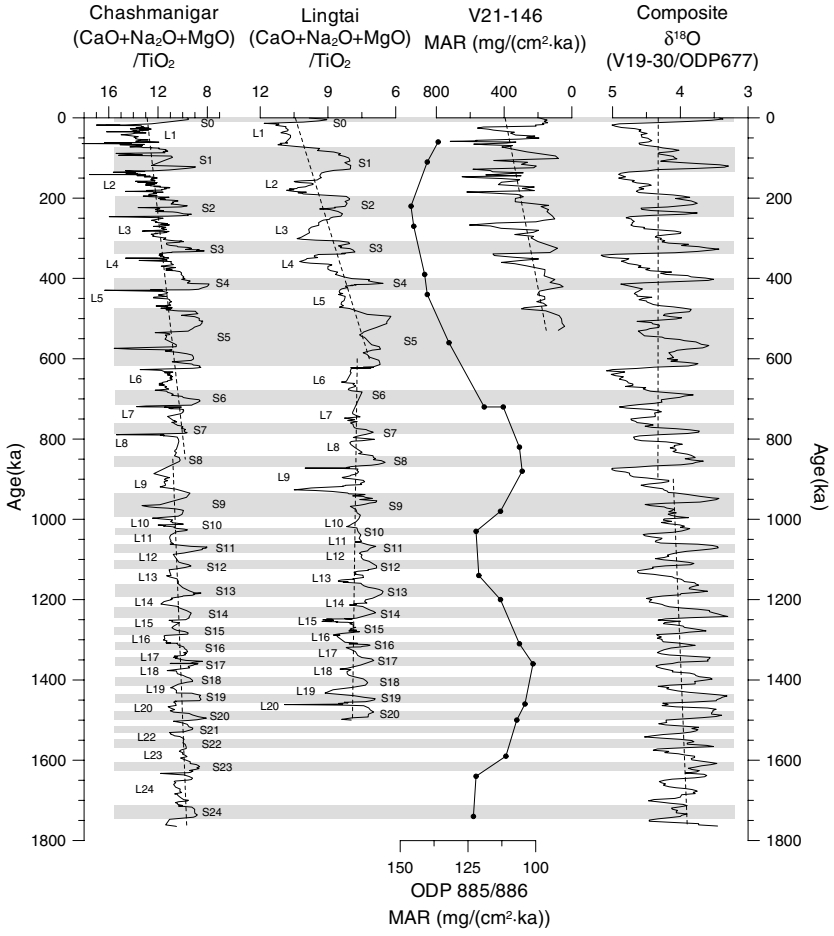

Fig. 15. Correlation of chemical weathering records of loess from China and Tajikistan with deep-sea eolian mass accumulation rate (MAR) records (V21-146, Hovan et al., 1991; ODP 885/886, Rea et al., 1998) and a composite marine oxygen isotope record. The $\delta^{18}O$ curve is a composite record of V19-30 (0–340 ka) (Shackleton and Pisias, 1985) and ODP 677 (340–1770 ka) (Shackleton et al., 1990). The dashed lines are linear fits of each curve for different time intervals. The shaded zones indicate interglacials.

$(CaO + Na_2O + MgO)/TiO_2$ ratios reflect a combination of chemical weathering in the source regions and the depositional areas. This may arise from two possible causes: namely, lowered maturity of clastic material in the source regions and lowered post-depositional weathering intensity.

There is evidence to support both explanations. Fe and Mg have increased since the mid-Pleistocene in both the Lingtai and Chashmanigar sections (Figs. 5 and 6). This is consistent with the gradual increase of unstable minerals (e.g., pyroxene and amphibole) in Chinese loess from the early to late Pleistocene (Liu, 1988), indicating increased fresh clastic materials in the source regions and/or a cooler and drier climate in the depositional areas. The higher dust sedimentation rate since 0.85–0.6 Ma in loess deposits, reflected by the thicker loess and soil units above S8 especially S5 soil unit (Figs. 3 and 4), and the oscillatory increase in eolian flux in North Pacific Ocean (Hovan et al., 1991; Rea et al., 1998) (Fig. 15), both suggest an increased aridity in Asian dust source regions since the mid-Pleistocene.

The decreased post-depositional weathering intensity is related to the shortened exposure time due to increased dust sedimentation rate (mentioned above) and the cooling and drying of climate conditions in the dust depositional regions. The deterioration of climate conditions around 0.85 Ma may be caused by the further increase of ice volume in northern hemisphere, as indicated by the ocean oxygen isotope record (Shackleton and Pisias, 1985; Shackleton et al., 1990) (Fig. 15). The mid-Pleistocene climate transition, characterized by a shift of dominant climatic periods from 41 to 100 ka at about 1.0–0.8 Ma, is clearly documented in both ocean oxygen record and loess deposits in China and Tajikistan, implying a close relationship between northern hemisphere ice and Asian loess deposition (Shackleton et al., 1995; Ding et al., 1995, 2002a,b). A recent study (Ding et al., 2005) suggests a stepwise weakening of the East-Asian summer monsoon since the late Pliocene, occurring at 2.6, 1.2, 0.7, and 0.2 Ma, which progressively reduced moisture transport from ocean to the Loess Plateau. However, glacial loess units are generally thought to be non-weathered or only slightly weathered in the depositional areas (Liu, 1988). Therefore, the rapid decrease of chemical weathering intensity of loess units since 0.85–0.6 Ma is more likely to reflect the lowered maturity of clastic

materials in the source regions. This may have resulted from two processes. First, expansion of northern hemisphere ice resulted in cooling and drying of Asian inland (e.g., Ding et al., 1995; Liu and Ding, 1998). Second, the regional tectonic uplift of high mountains (Li, 1991; Sun and Liu, 2000) produced abundant clastic materials for the dust source regions through enhanced denudation. In this context, both climate and tectonic forcing factors may be responsible for the decreasing chemical weathering intensity since the mid-Pleistocene.

It should be noted that the new proxy still reflects a mixed signal of weathering from both the source regions and the depositional areas, though it eliminates the grain-size effects to a large extent. An important future task is to develop proxies which can distinguish chemical weathering signal in source regions from that in depositional areas.

9. Conclusions

The major element and Rb, Sr, and Ba geochemistry of the north–south loess transect suggest that almost all elemental abundances and the currently used chemical weathering proxies such as CIA, Na_2O/Al_2O_3, Rb/Sr, and Ba/Sr vary considerably with changes in grain size. It was found that $(CaO + Na_2O + MgO)/TiO_2$ ratio of decarbonated residue is a robust proxy for chemical weathering intensity of loess deposits. The advantages of this proxy are that: (1) it appears independent of grain size, thus eliminating the influence of transport-driven differentiation of minerals to a large extent, (2) it reflects the comprehensive loss of elements for the loess deposits, and (3) it reflects chemical weathering intensity more reliably in dust deposits with large grain-size variations. The $(CaO + Na_2O + MgO)/TiO_2$ ratios of the Tajik and Chinese loess increase rapidly since 0.85–0.6 Ma, indicating that both the vast dust source regions and the depositional areas have undergone a decreasing chemical weathering intensity since the mid-Pleistocene. This event may be causally related to the expansion of northern hemisphere ice and/or the regional tectonic uplift of high mountains in Asia since the mid-Pleistocene.

Acknowledgments

This study is funded by the National Natural Science Foundation of China (Grants 40202016, 90202020, and 40021202) and the Chinese Academy of Sciences (KZCX2-SW-133). We are indebted to J. Quade and A. Reynolds for valuable comments and language improvement on an earlier version of this paper. We also thank S. Krishnaswami, E. Derbyshire, N. Rutter, and an anonymous reviewer for critical comments, V. Ranov, J.M. Han, and G.A. Wang for field assistance, and Z.Y. Gu for helpful discussions.

Associate editor: S. Krishnaswami

Appendix A. Supplementary data

Supplementary data associated with this article can be found, in the online version, at doi:10.1016/j.gca.2005.12.012.

References

An, Z.S., Kukla, G., Porter, S.C., Xiao, J.L., 1991. Late Quaternary dust flow on the Chinese Loess Plateau. *Catena* **18**, 125–132.

An, Z.S., Kutzbach, J.E., Prell, W.L., Porter, S.C., 2001. Evolution of Asian monsoons and phased uplift of the Himalaya-Tibetan plateau since Late Miocene times. *Nature* **411**, 62–66.

Chen, J., An, Z.S., Head, J., 1999. Variation of Rb/Sr ratios in the loess-paleosol sequences of central China during the last 130 000 years and their implications for monsoon paleoclimatology. *Quat. Res.* **51**, 215–219.

Ding, Z.L., Liu, T.S., Rutter, N.W., Yu, Z.W., Guo, Z.T., Zhu, R.X., 1995. Ice-volume forcing of East Asian winter monsoon variations in the past 800,000 years. *Quat. Res.* **44**, 149–159.

Ding, Z.L., Rutter, N.W., Liu, T.S., Sun, J.M., Ren, J.Z., Rokosh, D., Xiong, S.F., 1998. Correlation of Dansgaard-Oeschger cycles between Greenland ice and Chinese loess. *Paleoclimates* **2**, 281–291.

Ding, Z.L., Xiong, S.F., Sun, J.M., Yang, S.L., Gu, Z.Y., Liu, T.S., 1999. Pedostratigraphy and paleomagnetism of a ~7.0 Ma eolian loess-red clay sequence at Lingtai, Loess Plateau, north-central China and the implications for paleomonsoon evolution. *Palaeogeogr. Palaeoclimatol. Palaeoecol.* **152**, 49–66.

Ding, Z.L., Sun, J.M., Yang, S.L., Liu, T.S., 2001a. Geochemistry of the Pliocene red clay formation in the Chinese Loess Plateau and implications for its origin, source provenance and paleoclimate change. *Geochim. Cosmochim. Acta* **65**, 901–913.

Ding, Z.L., Yang, S.L., Sun, J.M., Liu, T.S., 2001b. Iron geochemistry of loess and red clay deposits in the Chinese Loess Plateau and implications for long-term Asian monsoon evolution in the last 7.0 Ma. *Earth Planet. Sci. Lett.* **185**, 99–109.

Ding, Z.L., Ranov, V., Yang, S.L., Finaev, A., Han, J.M., Wang, G.A., 2002a. The loess record in southern Tajikistan and correlation with Chinese loess. *Earth Planet. Sci. Lett.* **200**, 387–400.

Ding, Z.L., Derbyshire, E., Yang, S.L., Yu, Z.W., Xiong, S.F., Liu, T.S., 2002b. Stacked 2.6-Ma grain size record from the Chinese loess based on five sections and correlation with the deep-sea $\delta^{18}O$ record. *Paleoceanography* **17**, 1033. doi:10.1029/2001PA000725.

Ding, Z.L., Derbyshire, E., Yang, S.L., Sun, J.M., Liu, T.S., 2005. Stepwise expansion of desert environment across northern China in the past 3.5 Ma and implications for monsoon evolution. *Earth Planet. Sci. Lett.* **237**, 45–55.

Dodonov, A.E., 1991. Loess of Central Asia. *GeoJournal* **24**, 185–194.

Dodonov, A.E., Baiguzina, L.L., 1995. Loess stratigraphy of Central Asia: palaeoclimatic and palaeoenvironmental aspects. *Quat. Sci. Rev.* **14**, 707–720.

Domrös, M., Peng, G.B., 1988. *The Climate of China*. Springer, Berlin.

Eden, D.N., Wen, Q.Z., Hunt, J.L., Whitton, J.S., 1994. The mineralogical and geochemical trends across the Loess Plateau, North China. *Catena* **21**, 73–90.

Gallet, S., Jahn, B.M., Torii, M., 1996. Geochemical characterization of the Luochuan loess-paleosol sequence, China and paleoclimatic implications. *Chem. Geol.* **133**, 67–88.

Gallet, S., Jahn, B.M., Lanoë, B.V.V., Dia, A., Rossello, E., 1998. Loess geochemistry and its implications for particle origin and composition of the upper continental crust. *Earth Planet. Sci. Lett.* **156**, 157–172.

Garrels, R.M., Mackenzie, F.T., 1971. *Evolution of Sedimentary Rocks*. Norton & Company, New York.

Gu, Z.Y., Lal, D., Liu, T.S., Guo, Z.T., Southon, J., Caffee, M.W., 1997. Weathering histories of Chinese loess deposits based on uranium and

thorium series nuclides and cosmogenic ^{10}Be. *Geochim. Cosmochim. Acta* **61**, 5221–5231.

Gu, Z.Y., Ding, Z.L., Xiong, S.F., Liu, T.S., 1999. A seven million geochemical record from Chinese red-clay and loess-paleosol sequence: weathering and erosion in northwestern China. *Quat. Sci.* **4**, 357–365 (in Chinese with English abstract).

Guo, Z., Biscaye, P., Wei, L., Chen, X., Peng, S., Liu, T., 2000. Summer monsoon variations over the last 1.2 Ma from the weathering of loess–soil sequences in China. *Geophys. Res. Lett.* **27**, 1751–1754.

Hovan, S.A., Rea, D.K., Pisias, N.G., 1991. Late Pleistocene continental climate and oceanic variability recorded in northwest Pacific sediments. *Paleoceanography* **6**, 349–370.

Jahn, B.M., Gallet, S., Han, J.M., 2001. Geochemistry of the Xining, Xifeng and Jixian sections, Loess Plateau of China: eolian dust provenance and paleosol evolution during the last 140 ka. *Chem. Geol.* **178**, 71–94.

Ji, J.F., Chen, J., Lu, H.Y., 1999. Origin of illite in the loess from the Luochuan area, Loess Plateau, Central China. *Clay Miner.* **34**, 525–532.

Kukla, G., 1987. Loess stratigraphy in central China. *Quat. Sci. Rev.* **6**, 191–219.

Kukla, G., An, Z.S., 1989. Loess stratigraphy in central China. *Palaeogeogr. Palaeoclimatol. Palaeoecol.* **72**, 203–225.

Kukla, G., Heller, F., Liu, X.M., Xu, T.C., Liu, T.S., An, Z.S., 1988. Pleistocene climates in China dated by magnetic susceptibility. *Geology* **16**, 811–814.

Kutzbach, J.E., Guetter, P.J., Ruddiman, W.F., Prell, W.L., 1989. Sensitivity of climate to late Cenozoic uplift in southern Asia and the American West: numerical experiments. *J. Geophys. Res.* **94**, 18393–18407.

Li, J.J., 1991. The environmental effects of the uplift of the Qinghai-Xizang Plateau. *Quat. Sci. Rev.* **10**, 479–483.

Liu, T.S., 1988. *Loess in China*. Springer, Berlin.

Liu, T.S., Ding, Z.L., 1998. Chinese loess and the paleomonsoon. *Annu. Rev. Earth Planet. Sci.* **26**, 111–145.

Liu, T.S., Guo, Z.T., Liu, J.Q., Han, J.M., Ding, Z.L., Gu, Z.Y., Wu, N.Q., 1995. Variations of eastern Asian monsoon over the last 140,000 years. *Bull. Soc. Geol. Fr.* **166**, 221–229.

Loughnan, F.C., 1969. *Chemical Weathering of the Silicate Minerals*. Elsevier, New York.

Lydolph, P.E., 1977. *Climates of the Soviet Union*. Elsevier, Amsterdam.

Manabe, S., Broccoli, A.J., 1990. Mountains and arid climates of middle latitudes. *Science* **247**, 192–195.

Muhs, D.R., Bettis, E.A., Been, J., McGeehin, J.P., 2001. Impact of climate and parent material on chemical weathering in loess-derived soils of the Mississippi River valley. *Soil Sci. Soc. Am. J.* **65**, 1761–1777.

Nesbitt, H.W., Young, G.M., 1982. Early Proterozoic climates and plate motions inferred from major element chemistry of lutites. *Nature* **299**, 715–717.

Raymo, M.E., 1994. The initiation of northern hemisphere glaciation. *Annu. Rev. Earth Planet. Sci.* **22**, 353–383.

Rea, D.K., Snoeckx, H., Joseph, L.H., 1998. Late Cenozoic eolian deposition in the North Pacific: Asian drying, Tibetan uplift, and cooling of the northern hemisphere. *Paleoceanography* **13**, 215–224.

Ruddiman, W.F., Kutzbach, J.E., 1989. Forcing of late Cenozoic northern hemisphere climate by plateau uplift in southern Asia and the American West. *J. Geophys. Res.* **94**, 18409–18427.

Rutter, N.W., Ding, Z.L., Evans, M.E., Liu, T.S., 1991. Baoji-type pedostratigraphic section, Loess Plateau, north-central China. *Quat. Sci. Rev.* **10**, 1–22.

Shackleton, N.J., Pisias, N.G., 1985. Atmospheric carbon dioxide, orbital forcing, and climate. In: Sundquist, E.T., Broecker, W.S. (Eds.), *The Carbon Cycle and Atmospheric CO_2: Natural Variations, Archean to Present, Geophysical Monograph*, vol. 32. American Geophysical Union, Washington, DC, pp. 303–317.

Shackleton, N.J., Backman, J., Zimmerman, H., Kent, D.V., Hall, M.A., Roberts, D.G., Schnitker, D., Baldauf, J.G., Desprairies, A., Homrighausen, R., Huddlestun, P., Keene, J.B., Kaltenback, A.J., Krumsiek, K.A.O., Morton, A.C., Murray, J.W., Westberg-Smith, J., 1984. Oxygen isotope calibration of the onset of ice-rafting and history of glaciation in the North Atlantic region. *Nature* **307**, 620–623.

Shackleton, N.J., Berger, A., Peltier, W.R., 1990. An alternative astronomical calibration of the lower Pleistocene timescale based on ODP site 677. *Trans. R. Soc. Edinburgh Earth Sci.* **81**, 251–261.

Shackleton, N.J., An, Z.S., Dodonov, A.E., Gavin, J., Kukla, G.J., Ranov, V.A., Zhou, L.P., 1995. Accumulation rate of loess in Tadjikistan and China: relationship with global ice volume cycles. *Quat. Proc.* **4**, 1–6.

Sun, J.M., 2002. Provenance of loess material and formation of loess deposits on the Chinese Loess Plateau. *Earth Planet. Sci. Lett.* **203**, 845–859.

Sun, J.M., Liu, T.S., 2000. Stratigraphic evidence for the uplift of the Tibetan Plateau between ~1.1 and ~0.9 myr ago. *Quat. Res.* **54**, 309–320.

Taylor, S.R., McLennan, S.M., 1985. *The Continental Crust: its Composition and Evolution*. Blackwell, Oxford.

Wen, Q.Z., 1989. *Geochemistry of the Chinese Loess*. Science Press, Beijing (in Chinese).

Yang, J.D., Chen, J., Tao, X.C., Li, C.L., Ji, J.F., Chen, Y., 2001. Sr isotope ratios of acid-leached loess residues from Luochuan, China: A tracer of continental weathering intensity over the past 2.5 Ma. *Geochem. J.* **35**, 403–412.

Yang, S.L., Ding, Z.L., 2004. Comparison of particle size characteristics of the Tertiary 'red clay' and Pleistocene loess in the Chinese Loess Plateau: implications for origin and sources of the 'red clay'. *Sedimentology* **51**, 77–93.